A Novel Automatic Change Detection Method for Urban High-Resolution Remotely Sensed Imagery Based on Multiindex Scene Representation

Dawei Wen, Xin Huang, *Senior Member, IEEE*, Liangpei Zhang, *Senior Member, IEEE*, and
Jón Atli Benediktsson, *Fellow, IEEE*

Abstract—The new generation of Earth observation sensors with high spatial resolution can provide detailed information for change detection. The widely used methods for high-resolution image change detection rely on textural/structural features. However, these spatial features always produce high-dimensional data space since they are related to a series of parameters, e.g., window sizes and directions. Machine learning methods are also commonly employed, but their performances are subject to the quantity and quality of the training samples, and hence, much effort should be made to collect the high-quality samples. To address these problems, in this study, a novel multiindex automatic change detection method is proposed for the high-resolution imagery. The notable advantages of the proposed model include the following: 1) Complicated urban scenes are represented by a set of low dimensional but semantic information indexes, replacing the high-dimensional but low-level features (e.g., textural and structural features), and 2) the change detection model is carried out automatically without using training samples since the information indexes can directly indicate the primitive urban classes. The multiindex representation refers to the enhanced vegetation index, the water index, and the recently developed morphological building index. Experiments were conducted on the multitemporal WorldView-2 images over Shenzhen City (south of China) and Kuala Lumpur (the capital of Malaysia), where promising results were achieved by the proposed method. Moreover, the traditional methods based on the state-of-the-art textural/morphological features were also implemented for the purpose of comparison, which further validates the advantages of our proposed model.

Index Terms—Building detection, change detection, high resolution, morphological.

I. INTRODUCTION

DETECTION of land cover/use changes is one of the most fundamental and useful tasks for various applications such as urban expansion, urban planning, damage assessment, deforestation, and urban landscape monitoring [1]. With the rapid development of Earth observation techniques, it becomes convenient to obtain remotely sensed imagery over a certain area at different times. Thus, land cover/use changes can be effectively detected and analyzed by processing the multitemporal remote sensing images [2].

In recent years, change detection using high-spatial-resolution remote sensing images has received increasing interest since detailed ground change information is now available. However, a large intraclass variance and a small interclass variance can lead to inaccuracy for the traditional spectral-based and pixel-based image processing framework when high-spatial-resolution imagery is used for change detection [3]. In order to deal with this problem and improve the accuracy of change detection from high-resolution data, researchers have proposed to take spatial features into consideration for change detection, e.g., the gray-level cooccurrence matrix [4], wavelet transform [5], Markov random fields [6], morphological profiles [7], [8], and texton forest [9]. However, the spatial features are always related to a series of parameters such as window sizes, scales, and directions [10]. Therefore, traditional textural/structural feature extraction always leads to a high-dimensional feature space, which poses a series of problems when processing large-size data, e.g., the generalization and robustness of the methods, storage burden, computational cost, and processing efficiency.

On the other hand, some researchers proposed to use the machine learning methods for change detection. Camps-Valls *et al.* [11] introduced a multitemporal image classification and change detection framework based on composite kernels. Volpi *et al.* [8] adopted support vector machines in a supervised manner for change detection. In particular, semisupervised approaches have received much interest since it can achieve accurate results with limited training samples. Some representative examples refer to semisupervised Gaussian processes [12], a semisupervised multiple classifier system [13], and the modified self-organizing feature map neural network [14] for change detection.

It should be noted that, in recent years, a large number of remote sensing images can be acquired from hundreds of Earth observation platforms [15]. In order to timely process the big remote sensing data and rapidly transfer the data into information and knowledge, it is necessary to develop automatic techniques for image change detection. A few studies

have recently addressed the automatic change detection methods, including studies on multilevel change vector analysis [16], morphological filters with change vector analysis [7], multitemporal morphological attribute profiles [17], pulse-coupled neural networks [18], and hierarchical spectral change analysis [19].

In this paper, we propose a novel multiindex method for automatic change detection from high-spatial-resolution remotely sensed imagery over urban areas. The basic idea of the proposed method is to represent complicated high-resolution scenes by a set of low-dimensional semantic indexes that are used to replace traditional high-dimensional but low-level features (e.g., textural features and morphological profiles). Specifically, urban primitives, e.g., buildings, vegetation, and water, are automatically extracted by the morphological building index (MBI) [20], [21], the enhanced vegetation index (EVI), and the normalized difference water index (NDWI), respectively. Change detection can be then conveniently carried out by measuring the similarity between multitemporal multiindex histograms, represented by the frequency and spatial arrangement of the urban primitives. Moreover, the proposed method not only can detect binary change information, but it also indicates the types of changes, e.g., buildings, vegetation, and water.

This paper is organized as follows. The multiindex model for urban scene representation is introduced in Section II, followed by the proposed multiindex automatic change detection method in Section III. In Section IV, the data sets and the experimental results are presented. Some discussions are made in Section V. In Section VI, a comparative study is made between the proposed model and the change detection based on the state-of-the-art features. Section VII concludes this paper.

II. Multiindex Urban Representation

In this paper, three urban primitive indexes, i.e., MBI, EVI, and NDWI, are used to represent a typical urban scene. Please note that these three indexes provide information not only for buildings, vegetation, and water but also for nonbuildings, nonvegetation, and nonwater features, which actually enhances the discrimination ability of distinguishing different urban structures.

A. MBI

MBI is an effective method for automatic building detection. It is able to represent spectral–spatial properties of buildings (e.g., brightness, size, contrast, directionality, and shape) by a set of morphological operators. It should be noted that buildings are spectrally similar with the bright soil, and hence, the original MBI algorithm [20] is improved in this study by introducing a postprocessing step, aiming to reduce false alarms from the urban bright soil. The modified MBI algorithm is described as follows.

Step 1—Calculation of Brightness: The brightness is the maximum value of the visible bands for each pixel, which is used to represent the structures with high reflectance (e.g., candidate buildings). The visible bands are considered since they have the most significant contributions to the spectral reflectance of buildings [22].

Step 2—Top-Hat Morphological Profiles: Considering the fact that buildings and their spatially adjacent shadows lead to high local contrast, MBI is defined using differential morphological profiles (DMPs) [23], [24] of the white top-hat by reconstruction, i.e., DMP_{WTH}, as follows:

$$\text{DMP}_{\text{WTH}} = \{\text{DMP}_{\text{WTH}}(s, \text{dir}) : s_{\min} \leq s \leq s_{\max}, \text{dir} \in D\} \tag{1}$$

$$\text{DMP}_{\text{WTH}}(s, \text{dir}) = |\text{WTH}(s + \Delta s, \text{dir}) - \text{WTH}(s, \text{dir})| \tag{2}$$

where $\text{WTH}(s, \text{dir})$ represents the white top-hat of the brightness image obtained in step 1 by using a linear structural element (SE), with s and dir being the scale and the direction, respectively. $s_{\min}$ and $s_{\max}$ indicate the range of the spatial size of buildings, and Δs is the interval of the profiles. D is the set of directions for the linear SE.

Step 3: MBI is calculated by

$$\text{MBI} = \frac{\sum\limits_{s, \text{dir}} \text{DMP}_{\text{WTH}}(s, \text{dir})}{N_D \times N_S} \tag{3}$$

where N_D and N_S denote the number of directions and scales for the morphological profiles, respectively. Buildings correspond to the areas with high MBI values, due to their large local contrast in various directions and scales (please refer to [20] and [21] for details).

Step 4—Postprocessing: As aforementioned, in order to refine the result of the building detection, a postprocessing step is proposed to suppress the false alarms of bright soil from the original MBI. Spectral information plays a key role for identification of soil [25]. It should be noted that bright soil in an urban scene often has a yellow tone, corresponding to the urban construction sites. Therefore, based on the WorldView-2 images used in this study, a yellow soil index (YSI) can be defined using the normalized difference of yellow (Y) and blue (B) channels, i.e.,

$$\text{YSI} = \frac{\text{Y} - \text{B}}{\text{Y} + \text{B}}. \tag{4}$$

The reason why the yellow (band4) and blue (band2) bands are used to highlight the bright soil in urban areas is that soil in a typical urban scene shows a reflectance peak in the yellow channel but a relatively lower reflectance in the blue channel (see Fig. 1). On the other hand, the buildings show contrary reflectance properties to soil (i.e., reflectance peak in the blue but relatively lower reflectance in the yellow). Therefore, it is sensible to exploit the differences of reflectance between yellow and blue channels to indicate the yellow soil and, at the same time, suppress buildings in urban areas. Subsequently, the connected components with high YSI scores and large area values are identified as bright soil and removed from the MBI-based building detection result. Fig. 1 provides a graphic example for the improved MBI procedure, where the bright soil has been effectively removed from the initial building extraction.
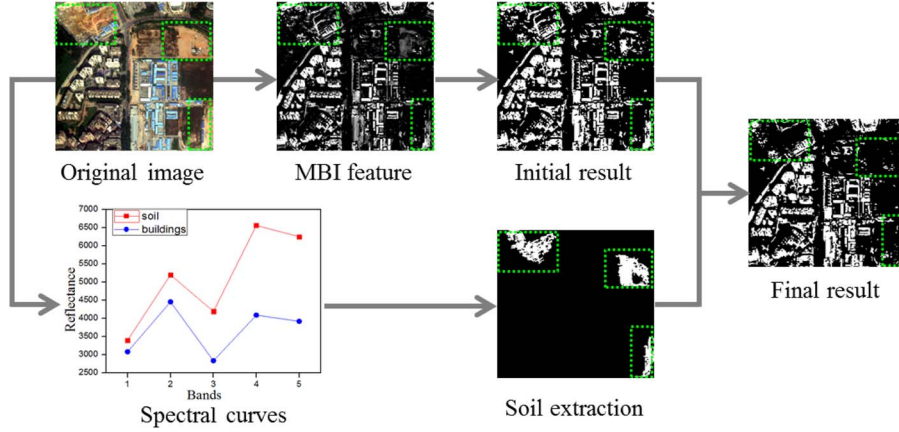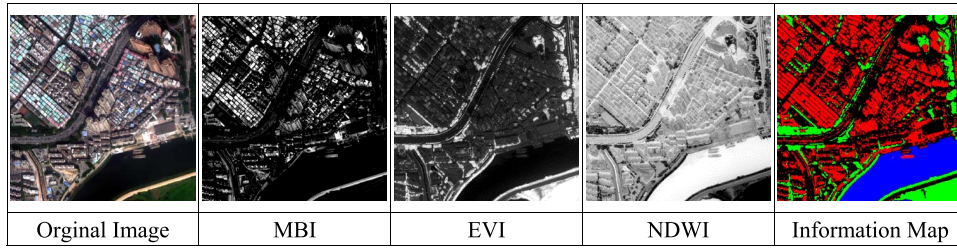
Fig. 1. Building detection procedure.

Fig. 2. Multiindex urban representation: Red = Buildings, Green = Vegetation, Blue = Water, Black = Ground (e.g., soil and roads).

B. EVI

The vegetation information is automatically extracted by the EVI [26], [27]. It was developed by enhancing the vegetation signals through the difference between near-infrared (NIR) and red (R) bands and, at the same time, reducing the aerosol effects using blue (B) band. EVI is defined as

$$EVI = 2.5 \frac{NIR - R}{NIR + 6R - 7.5B + 1}. \tag{5}$$

C. NDWI

The NDWI [28] is adopted to detect the water bodies. It highlights the water areas by maximizing the reflectance in green (G) band and minimizing the low reflectance in near-infrared (NIR) band, i.e.,

$$NDWI = \frac{G - NIR}{G + NIR}. \tag{6}$$

The water information is further refined by imposing an area-based threshold on the NDWI such that small noise and errors (e.g., shadows) can be removed.

An example is shown in Fig. 2, where a complicated high-resolution urban scene is represented by a set of information indexes (MBI, EVI, and NDWI). Subsequently, an information map can be obtained by simply applying a threshold to the indexes. It is clear that the urban primitive structures, such as buildings, shadow, vegetation, and ground, are effectively represented. Please note that this processing is automatically implemented without the need of collection of training samples. The threshold values for the MBI were chosen according to our

previous study [21], and the threshold values for water and vegetation indexes were determined by following the suggestions in [29] and [30].

III. AUTOMATIC CHANGE DETECTION

Based on the previous discussions, it can be stated that multiple information indexes have the potential for achieving automatic change detection from urban areas. Two examples for the multiindex automatic change detection are shown in Fig. 3, from which it is clearly seen that the structural changes in high-resolution images can be effectively indicated by the information indexes.

Here, a novel automatic change detection framework is proposed based on the multiindex model. The processing chain is demonstrated in Fig. 4. The notable characteristics of the multiindex method include the following aspects.

1) The complicated urban scenes can be automatically and effectively represented by a set of low-dimensional information indexes.
2) The local histograms of these indexes are able to describe the frequency and spatial arrangement of the urban primitives.

Consequently, the multitemporal multiindex representations can be used to detect the structural changes of the urban scenes. The proposed change detection method is described by the following steps.

Step 1—Calculation of Information Indexes: Information on buildings, vegetation, and water is obtained at the pixel level based on the MBI, the EVI, and the NDWI, respectively; and the corresponding postprocessing is then used to suppress

This article has been accepted for inclusion in a future issue of this journal. Content is final as presented, with the exception of pagination.

4   IEEE TRANSACTIONS ON GEOSCIENCE AND REMOTE SENSING
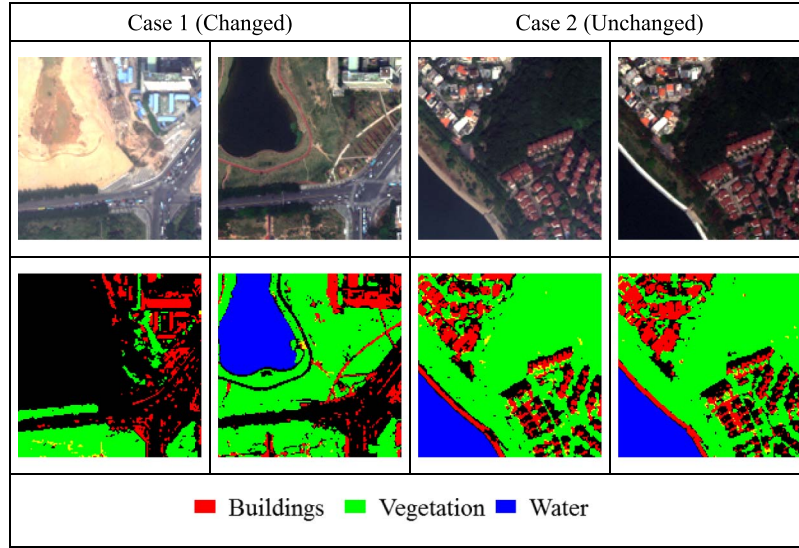

Fig. 3. Urban scene description based on the multiindex model. The first row shows the examples for the changed and unchanged scenes, respectively. The second row shows the corresponding information maps.
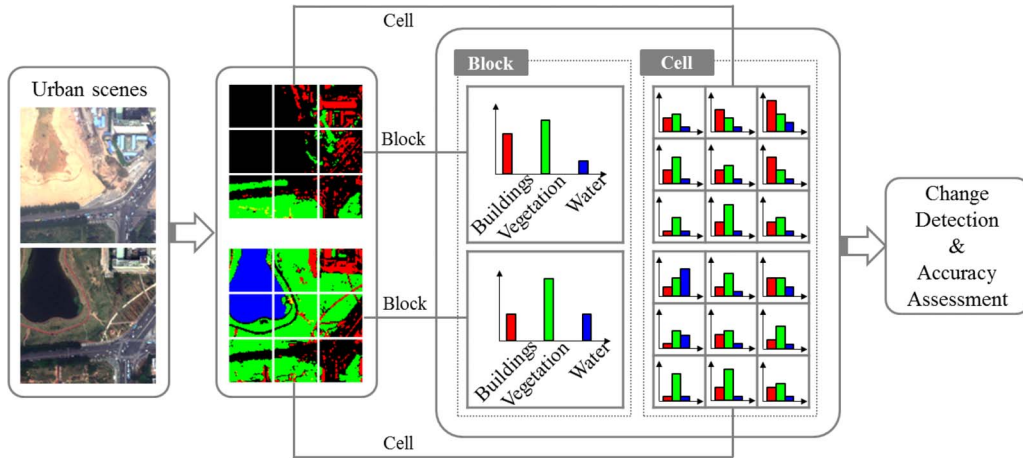

Fig. 4. Processing chain of the proposed multiindex change detection framework.

TABLE I
INFORMATION OF THE WORLDVIEW-2 IMAGES OVER SHENZHEN CITY USED IN THIS STUDY

	Wavelength (nm)	Coordinates	Size	Satellite angle zenith	Solar angle zenith
2010	Coastal: 400~450	Upper left coordinate:		153°	159°36′
	Blue: 450~510	22°37′13.16″N			
	Green: 510~580	114°2′29.99″E	6,433 ×		
	Yellow: 585~625		5,409 pixels		
2012	Red: 630~690	Lower right coordinate:	(140 km^2)	129°12′	138°30′
	Red Edge: 705~745	22°30′22.17″N			
	Near-infrared 1: 770~895	114°8′57.00″E			
	Near-infrared 2: 860~1040				

the noise in the initial result, i.e., removing bright soil from buildings and shadow from water bodies.

Step 2—Automatic Change Detection: The image is first divided into a series of blocks with the size of $N \times N$ (pixels) for each one, which is viewed as the basic unit for the change detection. This strategy is called "hot spot" detection [18], [31], which is a commonly used approach for change detection from high-resolution images. The decision for whether changes take place in this block is made according to the degree of similarity between the multitemporal multiindex histograms in the area. In this paper, two approaches, block based and cell based, are used to describe the multiindex distribution and measure the similarity.

a) Block-based strategy: In this case, the scene is represented by the frequencies of the primitives in the multiindex histogram of the block. For the block histograms at times T1 and

This article has been accepted for inclusion in a future issue of this journal. Content is final as presented, with the exception of pagination.

WEN *et al.*: CHANGE DETECTION METHOD FOR URBAN HIGH-RESOLUTION REMOTELY SENSED IMAGERY

5

T2, a weighted distance is used to determine whether changes occur in this area, i.e.,

$$\text{WDist} = \sum_{i=1}^{\text{Dim}} (\text{Dist}(i) \times \text{W}(i)) \tag{7}$$

$$\text{Dist}(i) = |H_1(i) - H_2(i)| \tag{8}$$

$$\text{W}(i) = \frac{\text{Dist}(i)}{\sum_{j=1}^{\text{Dim}} \text{Dist}(j)} \tag{9}$$

where WDist is the weighted distance between the histograms H_1 and H_2. Dim is the dimension of the histogram. $H_1(i)$ and $H_2(i)$ represent the frequency of the ith bin in the histograms H_1 and H_2, respectively. $\text{W}(i)$ is expressed as the normalized distance between $H_1(i)$ and $H_2(i)$, in order to further enlarge the difference for the dissimilar bins.

The block strategy describes the frequency of the multiindex primitives, but does not consider their spatial arrangement. Thus, in the second strategy, each block is further divided into a set of subblocks (called cells in the text), in order to depict the spatial distribution of the primitives.

b) Cell-based strategy: As shown in Fig. 4, spatial arrangement of the primitives can be considered by dividing each block into $n \times n$ cells. This way, a cell is viewed as a basic unit to calculate the frequencies of the information indexes. A block is then represented by $n \times n$ histograms, each one representing the frequencies of the multiindex features in each cell. Subsequently, the similarity measure between the bitemporal histograms is calculated, in order to determine whether changes occur in this block. In this case, the distance measure can be extended from (7), i.e.,

$$\text{WDist}_{\text{cell}} = \sum_{x=1}^{n \times n} \sum_{i=1}^{\text{Dim}} (\text{Dist}^x(i) \times \text{W}^x(i)) \tag{10}$$

$$\text{Dist}^x(i) = |\text{H}_1^x(i) - \text{H}_2^x(i)| \tag{11}$$

$$\text{W}^x(i) = \frac{\text{Dist}^x(i)}{\sum_{j=1}^{\text{Dim}} \text{Dist}^x(j)} \tag{12}$$

where $\text{H}_1^x(i)$ and $\text{H}_2^x(i)$ represent the frequency of the ith bin in the histogram for the xth cell ($1 \leq x \leq n^2$).

Step 3—Types of Change: It should be noted that most of the automatic change detection methods only indicate whether changes take place in the block but cannot provide specific information related to the types of changes. In this paper, however, based on the information indexes, it is possible to further provide the change information corresponding to each block, by investigating which information index is subject to significant changes in terms of both frequency and spatial arrangement in the block. This can be viewed as a by-product of the proposed change detection method.

IV. DATA SETS AND RESULTS

A. Data Sets

The study area covers Shenzhen City, which is one of the most developed cities in China. The area shows a typi-
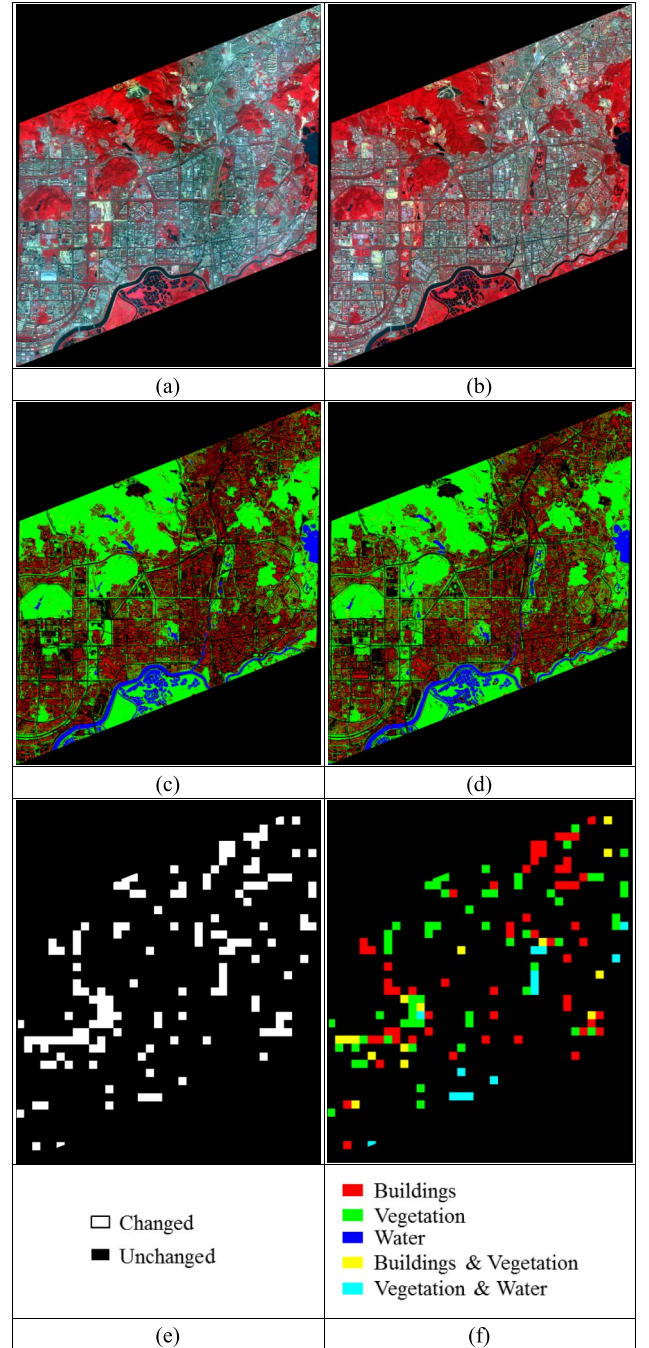

Fig. 5. WorldView-2 images over Shenzhen City. The images with false color composite (NIR-Green-Blue for RGB), acquired on November 3, 2010 and March 25, 2012, are shown in (a) and (b), respectively, as well as their corresponding multiindex representations in (c) and (d) (red = buildings, green = vegetation, and blue = water). (e) and (f) Ground truth for the binary change detection and the types of change, respectively.

cal Chinese urban landscape and land cover change pattern, e.g., the rapid urbanization and infrastructure construction. WorldView-2 multispectral images, consisting of eight multispectral bands with 2-m spatial resolution over Shenzhen City, are used in the experiments in order to test the change detection methods. Information for the images over the study area is provided in Table I. The bitemporal images, acquired on November 3, 2010 and March 25, 2012, respectively, are shown in Fig. 5(a) and (b), as well as the corresponding multiindex
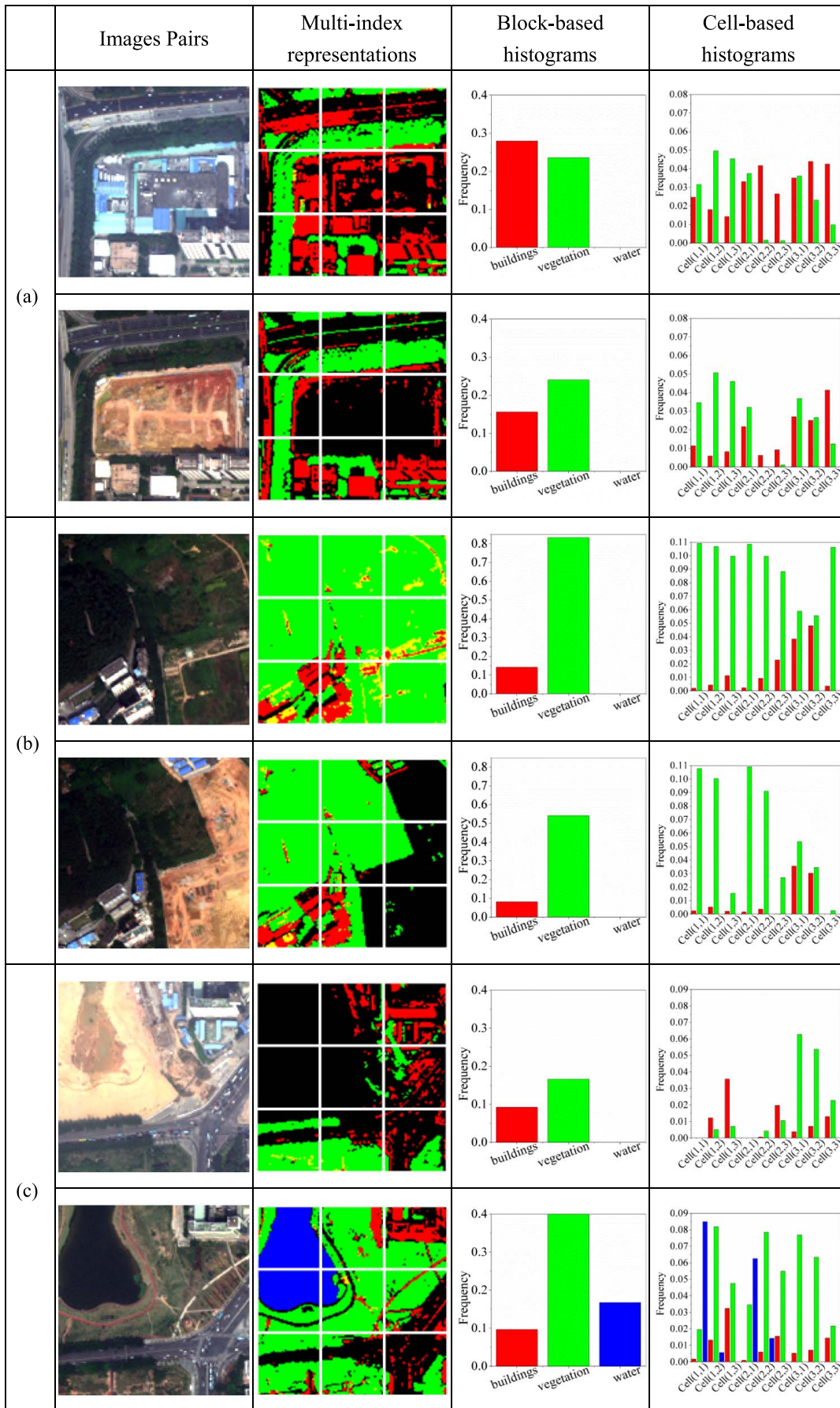
Fig. 6. Representative examples of the changed urban scenes and their block- and cell-based histograms. (a) Buildings. (b) Vegetation. (c) Water.

This article has been accepted for inclusion in a future issue of this journal. Content is final as presented, with the exception of pagination.

WEN *et al.*: CHANGE DETECTION METHOD FOR URBAN HIGH-RESOLUTION REMOTELY SENSED IMAGERY
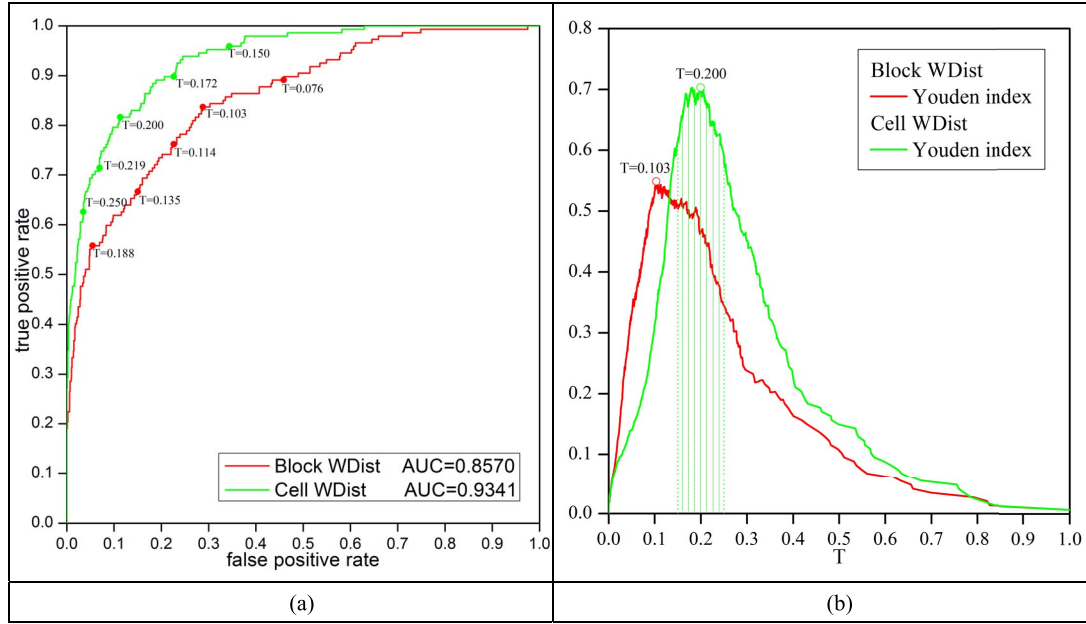7

Fig. 7. (a) and (b) ROC curves obtained by the proposed multiindex change detection models in the Shenzhen experiment. Some ROC points are associated to the corresponding threshold values "T," and in (b), the appropriate threshold values for the cell-based change detection are highlighted.

representations, displayed in Fig. 5(c) and (d). Fig. 5(e) and (f) shows the reference maps for binary change detection and the types of changes, respectively, which were manually generated based on a detailed field campaign and visual inspection. Please note that the legends in Fig. 5(f) indicate the changed classes in a block. For instance, "Building & Vegetation" means that the dominant source of change in a block refers to both buildings and vegetation.

Change information can be divided into seasonal changes and structural changes. The seasonal changes are always related to natural landscapes such as vegetation and water, whereas the structural changes could correspond to both natural and artificial objects. The changes in the study area are analyzed as follows.

1) Buildings: An example for changes of buildings is provided in Fig. 6(a). It is shown that the buildings in the middle of the block were removed, leading to a significant reduction of building components in both block- and cell-based histograms.

2) Vegetation: Please note that the seasonal effect for the vegetation can be ignored for the study area since the vegetation cover in Shenzhen City mainly refers to the evergreen plants, such as the South Asian tropical monsoon evergreen broad-leaved tree species [32]. Consequently, the changes of vegetation in this study area are only related to the structural changes caused by urban planning. A representative example is given in Fig. 6(b), where the vegetation was removed for the purpose of construction. The multitemporal changes are clearly reflected in the cell-based histograms in cell (1,3), cell (2,3), and cell (3,3), where a significant reduction of vegetation components can be observed.

3) Water: The changes of water in the urban areas can be related to both natural and artificial changes. An example for the artificial changes of the water is shown in Fig. 6(c), where a piece of soil land was changed into an artificial lake, leading

to a significant increment of water components in cell (1,1) and cell (2,1).

B. Results for the WorldView-2 Shenzhen Data Set

As aforementioned, the proposed multiindex change detection can provide two products.

1) Binary result: Each block is identified as changed or unchanged, which is the commonly used change detection strategy for high-resolution images [18], [33];
2) Change types: Based on the multiindex representation model, the proposed method can further indicate the types of changes in the block, e.g., buildings, vegetation, or water.

The quantitative accuracy for the binary change detection is measured by the receiver operating characteristic (ROC) [34] curves (see Fig. 7), where the vertical and horizontal axes, respectively, represent the true positive rate (TPR, hit rate) and the false positive rate (FPR, false alarm rate) calculated for all possible threshold values. Please note that, in a ROC curve, the point that is closest to the upper left corner is assumed to be an appropriate threshold value [e.g., $T = 0.103$ for block-based method and $T = 0.200$ for cell-based method, as marked in Fig. 7(a)], corresponding to relatively high detection accuracy and low false alarm. Furthermore, the area under the ROC curve (AUC) is often used to measure the overall accuracy of the detection method (a larger area corresponds to better result). In addition, the Youden index [35], which is defined as the difference between TPR and FPR (Youden index = TPR − FPR), is used to further quantitatively measure the accuracy of change detection. Larger values of the index correspond to better accuracy. The relationship between the thresholds and the Youden index is demonstrated in Fig. 7(b), which shows that reasonable threshold values range from 0.15 to 0.25 for the cell-based change detection.
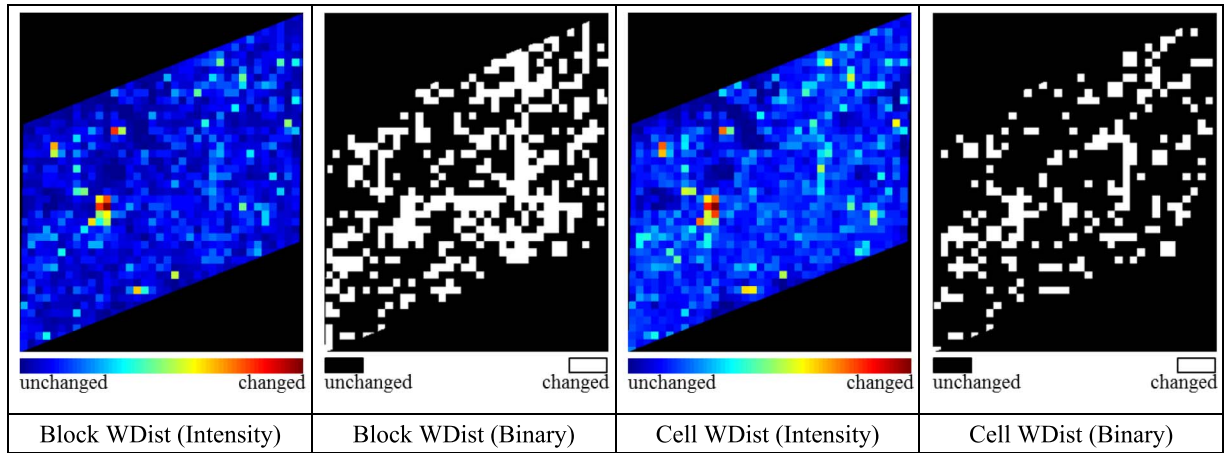
This article has been accepted for inclusion in a future issue of this journal. Content is final as presented, with the exception of pagination.

8   IEEE TRANSACTIONS ON GEOSCIENCE AND REMOTE SENSING

| Block WDist (Intensity) | Block WDist (Binary) | Cell WDist (Intensity) | Cell WDist (Binary) |

Fig. 8. Binary change detection results of the block/cell methods.
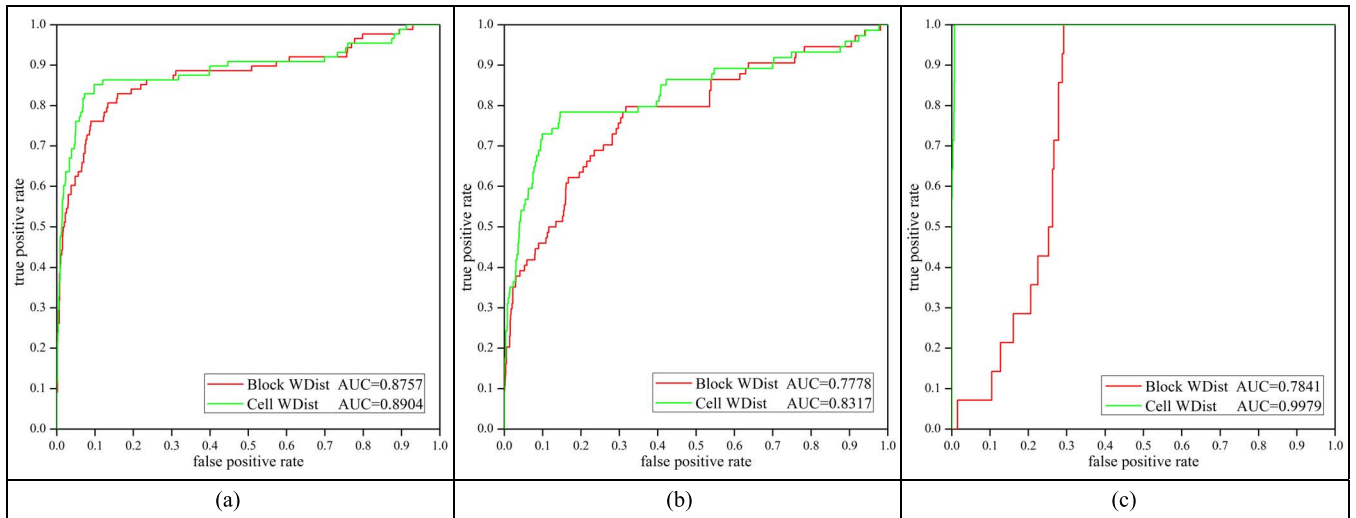
Fig. 9. ROC curves of change detection for (a) vegetation, (b) buildings, and (c) water.
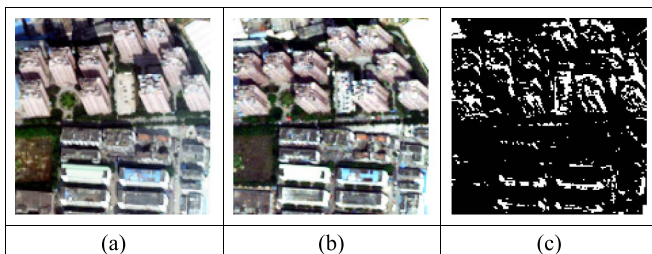

Fig. 10. Pixel-based change detection for the purpose of comparison. (a) 2010 image. (b) 2012 image. (c) Pixel-based change detection (change vector analysis).

In this experiment, each block is separated into 3×3 cells ($n = 3$). From the figures, we can obtain the following observations: The cell-based strategies provide much better results than the block-based ones since the accuracy curves show that, with the same FPR, the former can achieve much higher TPR than the latter. This phenomenon can be attributed to the fact that the cell-based strategy is able to simultaneously describe the frequency and spatial distribution of the urban multiindex primitives but the block-based strategy can only provide the frequency information.
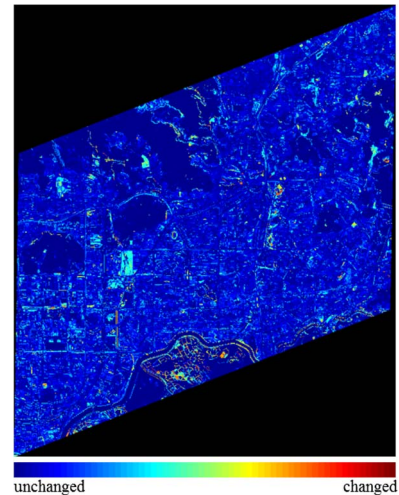

Fig. 11. Result of the object-based multiindex method.

The binary change detection results and the change intensity maps are displayed in Fig. 8, where the binary results are generated from the intensity maps by thresholding based on the ROC curves.

This article has been accepted for inclusion in a future issue of this journal. Content is final as presented, with the exception of pagination.

WEN *et al.*: CHANGE DETECTION METHOD FOR URBAN HIGH-RESOLUTION REMOTELY SENSED IMAGERY 9
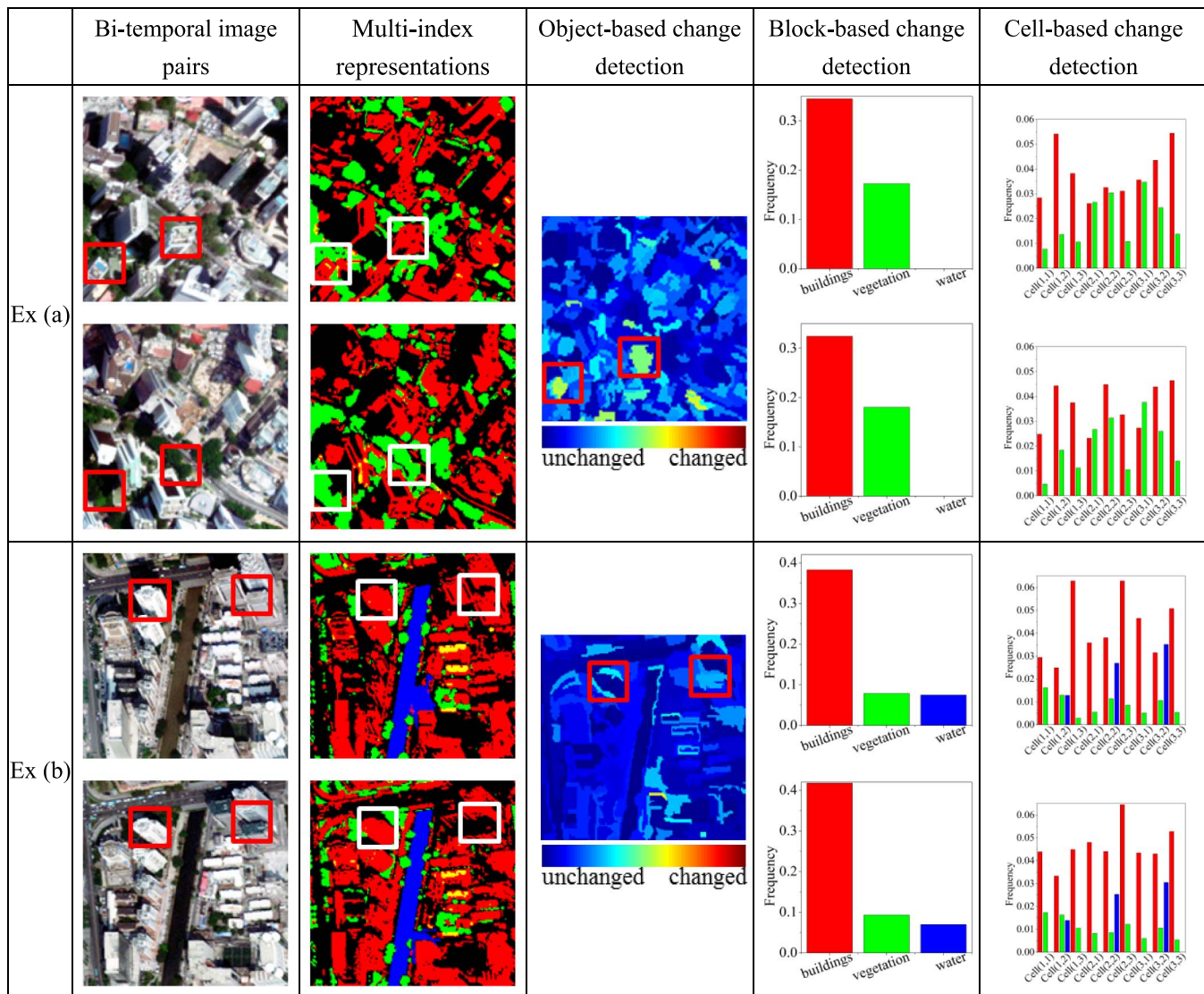

Fig. 12. Comparison of object-based and block- and cell-based change detection.

The accuracy for the change types is also assessed using the ROC curves. Fig. 9(a)–(c) corresponds to the accuracy curves for vegetation, buildings, and water, respectively. In general, it can be seen that the change detection accuracy for the vegetation and water is higher than the buildings by comparing their AUC values. This is understandable since EVI and NDWI are based on physical principles (e.g., photosynthesis for the vegetation), but MBI is based on the morphological assumptions of buildings. From Fig. 9, it is not surprising that, in all the cases (vegetation, buildings, water), the cell-based scene representation is much better than the block-based one, since the former takes the spatial arrangement of the multiindex primitives into consideration.

V. DISCUSSION

Here, some important and interesting issues about the proposed scene-based (i.e., block and cell) change detection are discussed.

A. Comparison With the Pixel-Based Change Detection

The experimental results show that the cell-based multiindex scene representation can achieve accurate change detection from urban high-resolution images. An interesting example is provided in Fig. 10, where no significant changes happen in this scene. It should be kept in mind that the multitemporal representation for remote sensing imagery is difficult and complicated for the high-spatial-resolution images. For instance, a building can be related to multiple imaging parameters, e.g., viewing angle, adjacent shadow, and the solar zenith angle. An unchanged building could be incorrectly identified as changed when these parameters are significantly different for multitemporal images. Consequently, the pixel-based change detection methods always lead to a large number of false alarms, as shown in Fig. 10(c). The result in Fig. 10(c) is obtained using the pixel-based change vector analysis method with Otsu's automatic threshold [36]. This example shows that the block- and cell-based change detection is more appropriate for the high-resolution image change detection, since it is able to tolerate
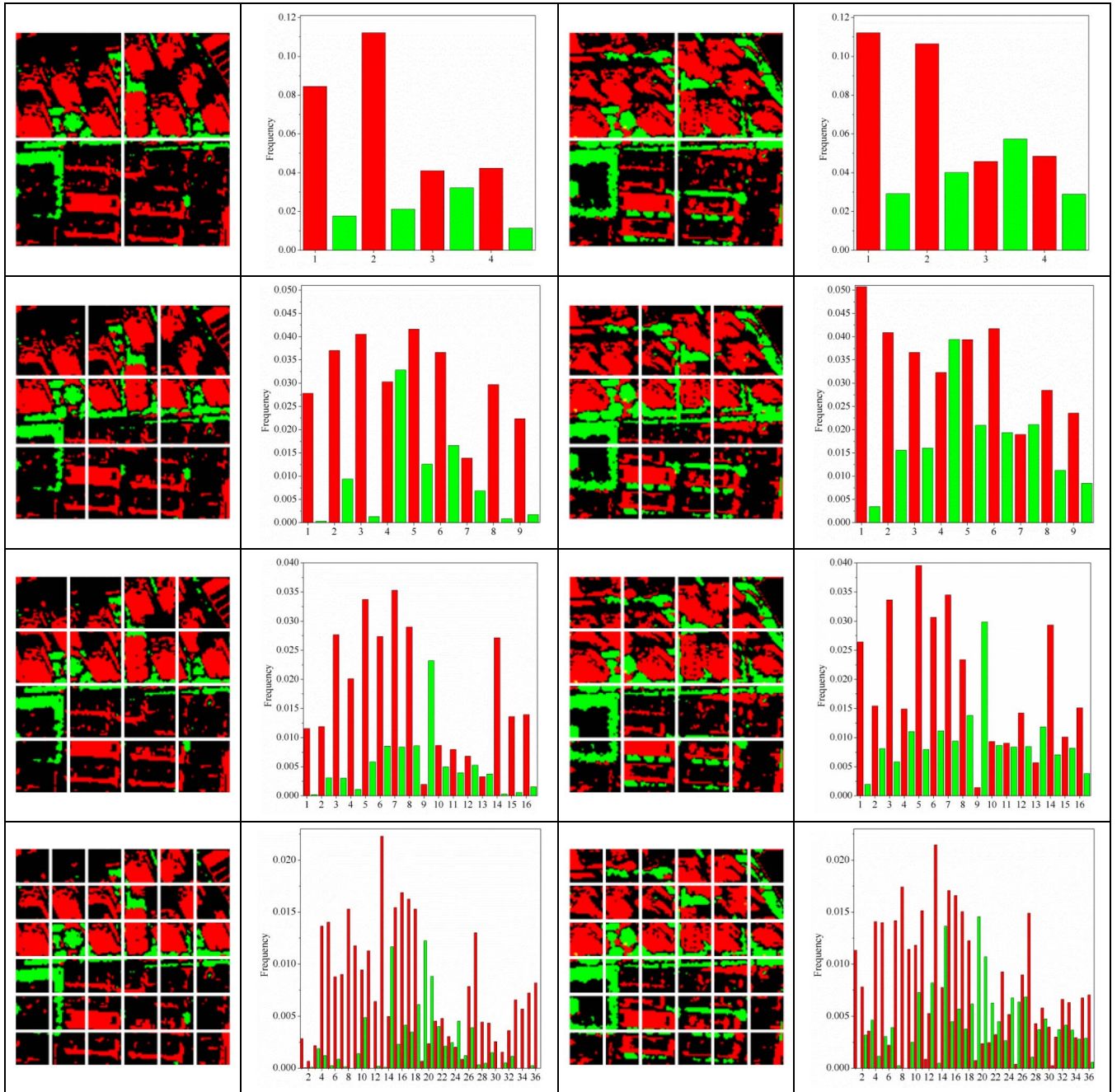
Fig. 13. Cell-based histogram representation with different sizes (2×2, 3×3, 4×4, and 6×6).

the spatial differences resulting from the different imaging parameters of the multitemporal data sets.

B. Comparison With the Object-Based Change Detection

The object-based multiindex method was implemented to make a comparison with our block- and cell-based methods. The object-based change detection is carried out according to [16] and [37], with the multiple information indexes used as features. The result of the object-based change detection is displayed in Fig. 11.

Several examples are presented in Fig. 12 to further show the difference between the object-based change detection and the proposed block- and cell-based methods. It can be seen that a lot of false alarms were identified by the object-based change detection, due to the significant geometrical difference between bitemporal images (e.g., viewing angles). However, on the other hand, the scene was identified as an unchanged one by the proposed methods since the difference between the bitemporal histograms is small.

C. Influence of the Number of Cells

The key parameter for the cell-based method is the number of cells ($n \times n$) in each block. Fig. 13 shows a series of cell-based multiindex scene representations with different values of n ($n = 2, 3, 4, 6$). It can be clearly seen that the cell-based histograms become more sensitive to the imaging parameters
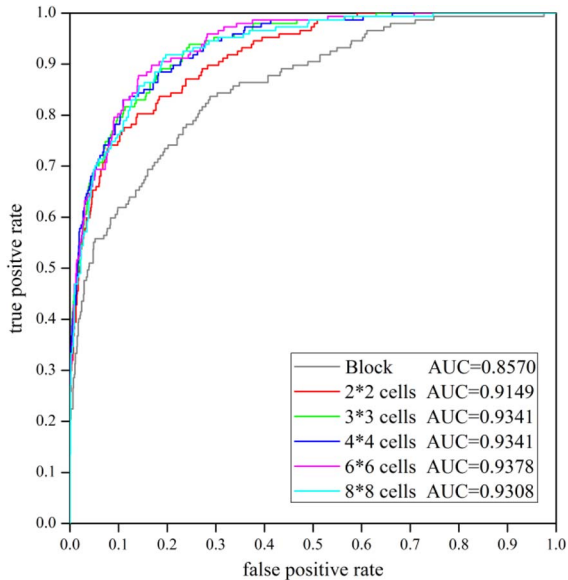
This article has been accepted for inclusion in a future issue of this journal. Content is final as presented, with the exception of pagination.

WEN *et al.*: CHANGE DETECTION METHOD FOR URBAN HIGH-RESOLUTION REMOTELY SENSED IMAGERY 11

Fig. 14. ROC curves obtained by the cell-based multiindex change detection method with different configurations of cells (2×2, 3×3, 4×4, 6×6, and 8×8).

(e.g., viewing angle, adjacent shadow, and the solar zenith angle) when the value of n (number of the cells in a block) increases. An extreme case is the pixel-based change detection [see Fig. 10(c)], where a cell actually corresponds to a pixel in the block. This way, the results are subject to a large number of commission errors caused by the different imaging conditions of the bitemporal images. In order to quantitatively show the influence of the parameter n, the ROC curves with different configurations of cells (2×2, 3×3, 4×4, 6×6, and 8×8) are compared in Fig. 14. It can be found that the 3×3, 4×4, 6×6, and 8×8 cells achieved similar and satisfactory results in terms of the ROC curves, outperforming the 2×2 and block-based (1×1) approaches. On one hand, a large value of n can describe the structural arrangement of primitives in a scene more adequately. On the other hand, however, a large value of n may lead to overrepresentation of an image scene, which needs more complex computation but does not improve the performance significantly. Thus, a 3×3 cell configuration is employed in this research.

D. Observation of Errors

Although the proposed methods are effective in indicating most of the changes taking place in the study area, it led to a few errors due to the spatiotemporal complexity of the multitemporal urban high-resolution scenes. In spite of this, the errors are within a tolerant range since the change detection is carried out without collection of training samples and human–computer interaction. Several cases of observations are chosen for showing the errors of the proposed methods. Here, the cell-based strategy with weighted distance is taken as an example for the error analysis.

Case 1 [see Fig. 15(a)] is related to a commission error caused by the effect of the viewing angles and the solar zenith angles, which are significantly different between the 2010 and 2012 images. In particular, please pay attention to the rectangular region, where the difference of the shadow led to a structural change.

Case 2 corresponds to an omission error of buildings [see Fig. 15(b)]. Focusing on the highlighted area, it can be seen that a piece of bare land was changed into buildings. However, the bare land was incorrectly identified as a building by the MBI algorithm in the 2010 image. This case reveals that although YSI is able to suppress most of the false alarms for the bright soil, some errors still exist.

Case 3 is an interesting example of an omission error [see Fig. 15(c)]. In the rectangular region, it can be observed that a factory was newly built near the water body in 2012, leading to degradation of the water quality in the region due to the sewage discharge. Thus, the water was not detected by the NDWI in 2012. This change is clearly shown in the multiindex features. Unfortunately, it has not been identified by the proposed method since the changed components were not identified as a change by the threshold value selected. The threshold value is marked in Fig. 7, which was selected considering the balance between detection rate and false alarm rate.

E. Additional Data Set

In order to test the robustness of the proposed scene-based change detection, another WorldView-2 data set over Kuala Lumpur (capital of Malaysia) was added to evaluate our proposed method. The bitemporal images and the ground truth map and detection result are provided in Fig. 16. The imaging parameters (i.e., satellite angle zenith and solar angle zenith) of the Kuala Lumpur images are given in Table II. As shown in the table, the imaging parameters of the Kuala Lumpur bitemporal images are significantly different, which pose a challenge to the tolerance of the proposed method for the multitemporal geometrical differences. In spite of this, from the change detection results in Fig. 17 and ROC curves shown in Fig. 18, it can be seen that the proposed multiindex model can also achieve satisfactory results with the additional data set.

F. Thresholding Strategies

The thresholding strategy is a key step for automatic change detection to generate the change map. In the previous experiments, the suitable threshold values [marked in Figs. 7(a) and 18(a)] were selected based on the ROC curves, corresponding to a high detection rate and a low false alarm. In addition, a suitable threshold value can be estimated by the following strategies.

1) Suggested threshold values: The suitable values for the cell-based change detection range from 0.15 to 0.25, in terms of the two experiments in this study [see Figs. 7(b) and 18(b)]. The best points for both experiments are close to $T = 0.2$.

2) Automatic threshold: Automatic thresholding methods, e.g., Otsu's [36] and minimum cross entropy (MCE) [38], can be applied to estimate the appropriate threshold values. Their results are reported in Table III. It can be found that the MCE is able to give a satisfactory result in terms of the accuracy (Youden index).
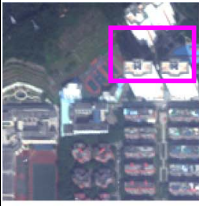
This article has been accepted for inclusion in a future issue of this journal. Content is final as presented, with the exception of pagination.

12   IEEE TRANSACTIONS ON GEOSCIENCE AND REMOTE SENSING
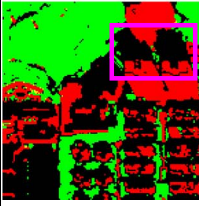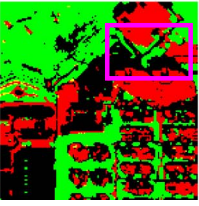
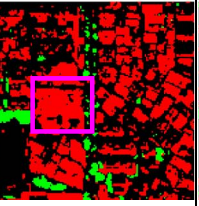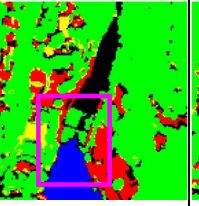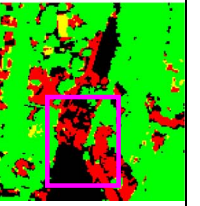| (a) A commission error		(b) An omission error		(c) An omission error	
2010	2012	2010	2012	2010	2012

| The difference of the viewing angles and the solar zenith angles between the two images led to the comission error. | The misclassification between bare soil and buildings by the MBI algorithm led to this omission. | The threshold setting for the change detection led to this omission error. |

Fig. 15. Error analysis for the proposed method by taking the cell-based strategy with weighted distance measure as an example.
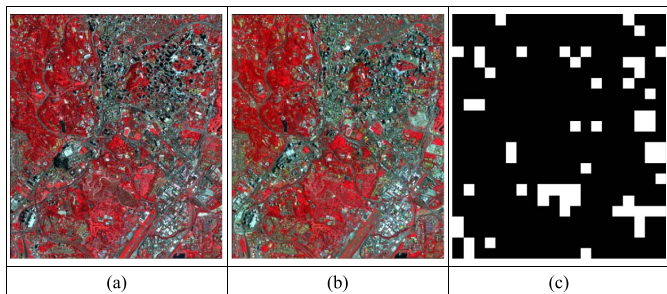

Fig. 16. WorldView-2 images over Kuala Lumpur city. The images acquired on February 17, 2011 and June 27, 2014, are shown with false color composite (NIR-Green-Blue for RGB) in (a) and (b), respectively. (c) Ground truth map for binary change detection (white = changed, black = unchanged).

TABLE II
IMAGING PARAMETERS OF THE WORLDVIEW-2
IMAGES OVER KUALA LUMPUR

Images	Satellite angle zenith	Solar angle zenith
Kuala Lumpur (2011)	226°48′	127°36′
Kuala Lumpur (2014)	335°24′	39°6

VI. COMPARISON BETWEEN MULTIINDEX AND TRADITIONAL FEATURES

The proposed multiindex representation is a high-level image description approach, i.e., an image scene is represented using a set of information indexes, which can directly indicate the basic urban classes (e.g., vegetation, water, buildings, and ground). This concept is quite different from traditional methods, which are related to high-dimensional but low-level feature representation (e.g., textures, morphology, and shape). Thus, a comparative study between the proposed model and the traditional methods (i.e., textural/morphological features) is conducted in order to show the superiority of the multiindex change detection model from the feature representation point of view.

In the multifeature methods, a series of state-of-the-art spatial features are used for the urban scene description and the subsequent change detection. In order to guarantee a fair comparison, the comparative study is carried out similarly to the proposed method. The change or no-change is determined according to the similarity of the multifeature histograms between the time T1 and T2. As shown in Fig. 19, the processing chain refers to three steps: feature extraction, scene representation, and change detection.

1) Feature Extraction: The spatial features considered for comparison are briefly introduced as follows.

Occurrence statistics [39]: Two occurrence measures, i.e., local mean and variance, are computed on the basis of gray-level values within a moving window centered on each pixel.

Cooccurrence statistics [40]: Gray-level cooccurrence matrix (GLCM) is one of the most commonly used textural features for remote sensing texture analysis. It defines a series of statistical features by recording the frequencies of two neighboring pixels that occur in a certain distance and angle. In this paper, according to [41] and [42], three widely used textural measures, i.e., entropy (ENT), homogeneity (HOM), and contrast (CON), are used in the comparative study to describe the urban scenes.

In the experiment, three window sizes, i.e., 3×3, 7×7, and 15×15, are chosen for computation of the occurrence and cooccurrence textural measures, by considering the spatial resolution and the sizes of the objects in the study area. In addition, the directional effects of the cooccurrence textural features are removed by taking the average value of the extracted features over four directions ($0°$, $45°$, $90°$, and $135°$). The offset parameters of GLCM are defined as follows: 1 pixel shift for 3×3, 2 pixels for 7×7, and 4 pixels for 15×15, according to the suggestions in [8].

Morphological attribute features: Recently, the morphological attribute profiles (APs) [43] have received much attention and proved to be effective for classification [43], [44] and
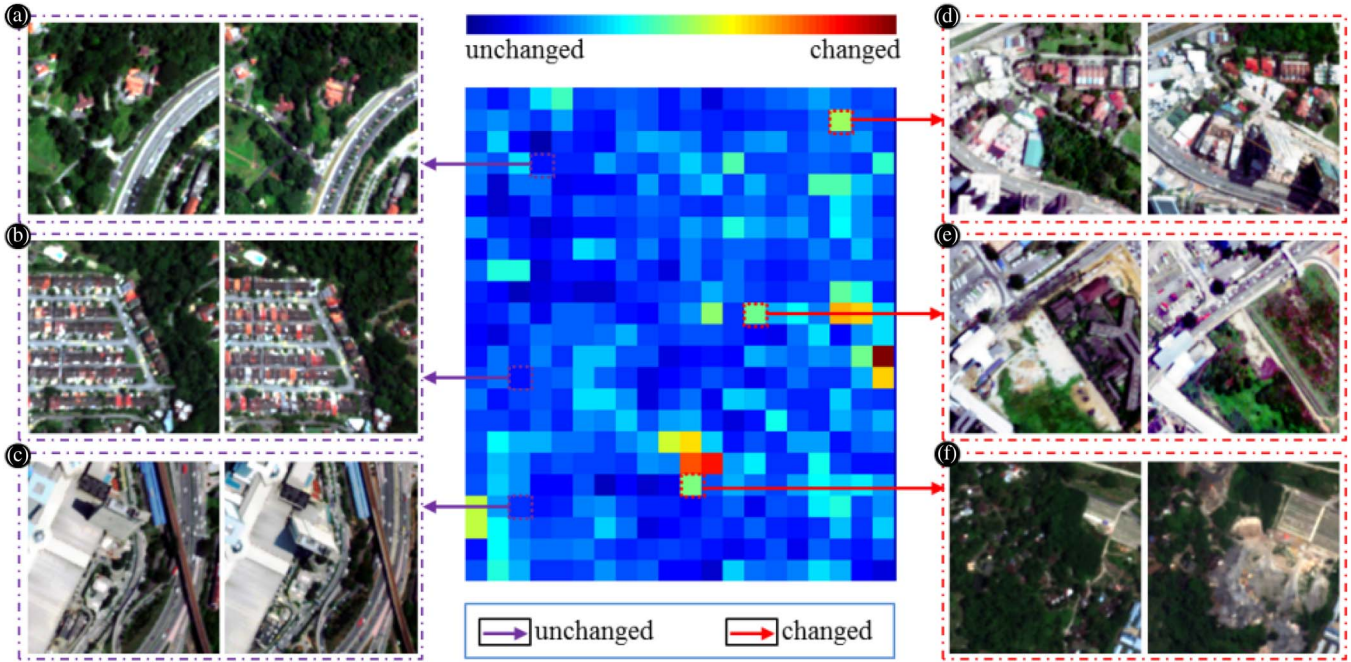
Fig. 17. Change detection results and several examples: unchanged blocks (A, B, and C) and changed blocks (D, E, and F).
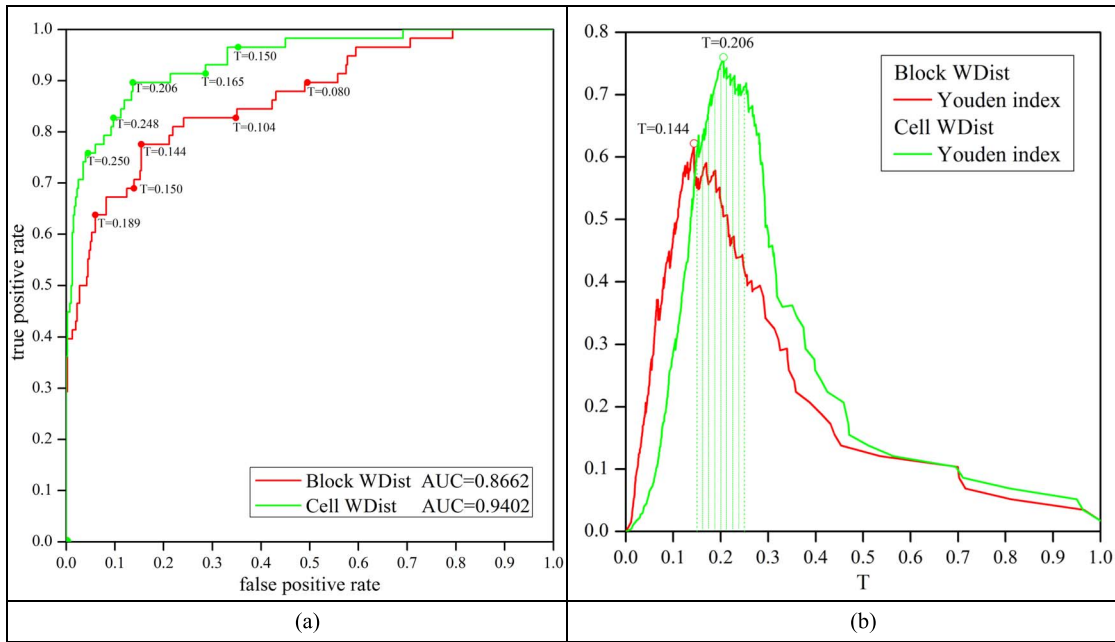

Fig. 18. (a) and (b) ROC curves achieved by the proposed multiindex change detection models in the Kuala Lumpur experiment. Some ROC points are associated to the corresponding threshold values "T," and in (b), the appropriate threshold values for the cell-based change detection are highlighted.

TABLE III
COMPARISON OF DIFFERENT THRESHOLDING STRATEGIES
FOR THE CELL-BASED CHANGE DETECTION

	Strategy	Threshold	TPR	FPR	Youden index
Shenzhen	ROC	$T = 0.200$	0.8163	0.1132	0.7031
	Otsu's	$T = 0.110$	0.9932	0.6197	0.3735
	MCE	$T = 0.181$	0.8844	0.1827	0.7017
KL	ROC	$T = 0.206$	0.8966	0.1368	0.7598
	Otsu's	$T = 0.377$	0.3103	0	0.3103
	MCE	$T = 0.234$	0.7931	0.0846	0.7085

change detection [17] from high-resolution images. Therefore, in this study, APs are considered for comparison. APs are extended from the morphological profiles by replacing the opening and closing operators with a series of morphological attributes in a multilevel way. Specifically, APs are constructed based on the attribute thinning and thickening operators. APs can be calculated with a series of scale-based threshold values (λ). Four morphological attributes are considered in this paper, and their parameters are defined according to [43]: 1) area of the regions ($\lambda_a = [100\ 500\ 1000]$);

This article has been accepted for inclusion in a future issue of this journal. Content is final as presented, with the exception of pagination.

14   IEEE TRANSACTIONS ON GEOSCIENCE AND REMOTE SENSING
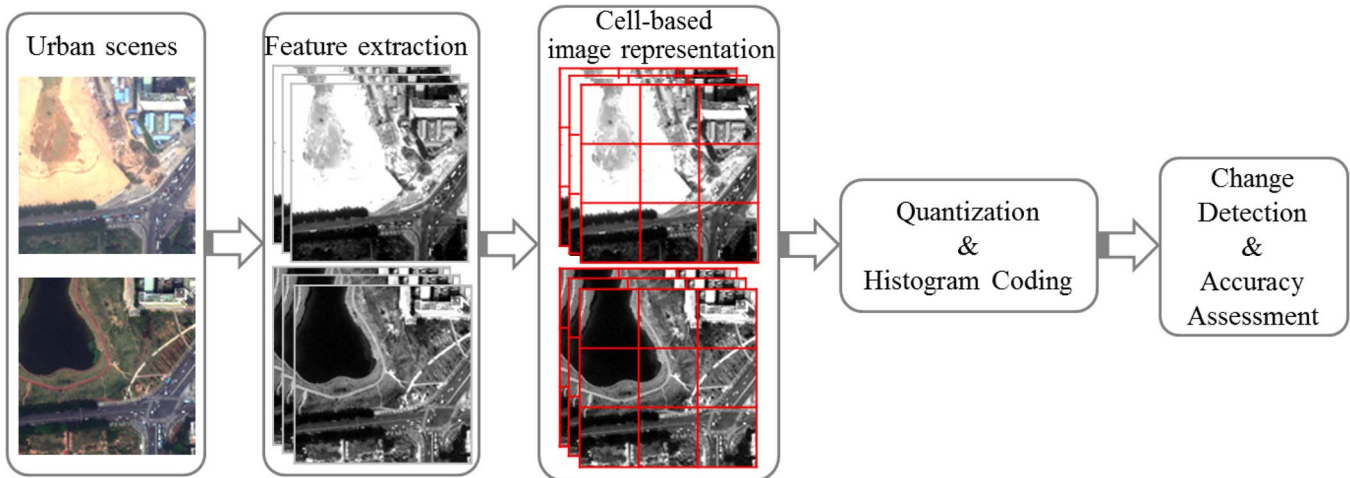

Fig. 19. Processing flow of the multifeature change detection for the purpose of comparison.

TABLE IV
COMPARISON OF THE CHANGE DETECTION RESULTS BETWEEN THE MULTIFEATURE METHODS AND THE PROPOSED MULTIINDEX METHODS
(DIM = DIMENSION OF THE HISTOGRAM, SPEC = SPECTRAL BANDS, OC = OCCURRENCE TEXTURES)

Methods	Features	TPR (with FPR=0.15)	AUC	Dim (n=3)
	Spec	0.0952	0.5026	$8\times10\times n^2$=720
Traditional	OC	0.2585	0.6585	$6\times10\times n^2$=540
Multi-feature methods	GLCM	0.0612	0.4617	$9\times10\times n^2$=810
	Spec + OC + GLCM	0.1156	0.4872	$23\times10\times n^2$=2070
	APs	0.3537	0.6998	$26\times10\times n^2$=2340
The proposed	Block (WDist)	0.6667	0.8570	3
Multi-index methods	Cell (WDist)	0.8299	0.9341	$3\times n^2$=27

2) length of the diagonal of the bounding box ($\lambda_d = [10\ 25\ 50\ 100]$); 3) the first moment of inertia ($\lambda_i = [0.2\ 0.3\ 0.4\ 0.5]$); and 4) standard deviation ($\lambda_s = [20\ 30\ 40\ 50]$).

2) Cell-Based Scene Representation: This step is similar to the proposed multiindex change detection. An image is divided into a series of blocks ($N \times N$ pixels), and each block is further separated into $n \times n$ cells ($n = 3$). Subsequently, the histograms for the features are generated by quantizing the features into ten bins (the quantization level) for each cell. In a similar way, each block is represented by stacking the feature histograms of all the cells within it.

3) Automatic Change Detection: The cell-based distance $\text{Dist}_{\text{cell}} = \sum_{x=1}^{n \times n} \sum_{i=1}^{\text{Dim}} \text{Dist}^x(i)$ is used here to measure the similarity of the multitemporal and feature histograms and then determine whether changes take place in the block. Please note that the traditional feature representation is only able to provide the information for change or no-change, but not able to indicate which kind of land cover class changes in the area.

The accuracies of the multifeature and multiindex change detection are compared in Table III, where various feature combinations are tested. The table shows that the accuracies obtained by the multifeature methods are not satisfactory. APs achieved the best result among the traditional multifeature methods with TPR = 0.3573 and AUC = 0.6998. However, with the same FPR (FPR = 0.15), the proposed multiindex change detection model can achieve significantly higher TPR (TPR = 0.8299) and AUC (AUC = 0.9341). A sensible explanation to this phenomenon is that the proposed multiindex model can directly represent the urban primitives with the information indexes (e.g., buildings, vegetation, and water), but traditional methods use low-level textural and morphological features, which is actually an indirect description of structures in the image scenes. There is a semantic gap between the low-level features and the high-level semantics for image understanding [45], [46]. The proposed multiindex model is able to achieve image semantic description by modeling the frequency and the distribution of a set of basic urban primitives. Instead, traditional textural and morphological features fail to describe the image semantics directly. Moreover, another notable advantage of the multiindex representation is that the histogram dimensionality (Dim) of each block is much smaller than that for the traditional low-level feature representation (see Table IV), and hence, the proposed approach needs less storage space and computational cost.

VII. CONCLUSION

In this paper, an innovative change detection method based on the multiindex image representation has been proposed for high-resolution remote sensing imagery over urban scenes. The proposed method is capable of achieving satisfactory change detection accuracy with a set of low-dimensional but semantic information indexes, e.g., MBI, EVI, and NDWI. Two specific strategies are implemented for the proposed method. The first one is a block-based approach, where the frequencies of the

information indexes are considered for change detection. The other is the cell-based one, where each block is further separated into a series of cells. This way, not only the frequencies but also the spatial arrangement of the information indexes in the block can be exploited. In experiments, it was found that the cell-based approach significantly outperformed the block-based one for both binary and class-specific change detection. This phenomenon reveals that the order or arrangement of the primitives in a scene plays a key role for the scene-based image interpretation.

A comparative study was conducted between the proposed multiindex method and the traditional multifeature method for automatic change detection. Some widely used and state-of-the-art spatial features were considered, including GLCM textures and morphological APs. The comparison demonstrates that the proposed multiindex model can achieve significantly better performance than the traditional multifeature methods, since the former gave much higher correctness score with the same false alarm rate. Results also showed the superiority of the proposed multiindex representation for scene interpretation, compared with the traditional high-dimensional and low-level features. The information indexes can directly reflect the basic semantic components of the imagery, and their spatial arrangement can be used to model the configurations of the scenes. In addition, the proposed multiindex model can automatically indicate which class the change in the area is related to. This is a by-product of the proposed method. Instead, traditional automatic change detection can only determine whether changes take place in this region or not.

Additionally, the object-based multiindex method was conducted to make the comparison with our proposed methods. It can be seen that the object-based method may suffer from a number of false alarms caused by the geometrical difference between the bitemporal high-resolution images (e.g., different viewing angles). However, this kind of false alarm can be effectively suppressed by the proposed block/cell method, due to the tolerance of the multiindex histograms to the geometrical differences.

In future research, we plan to validate the proposed change detection method in more urban areas with high-resolution images and attempt to implement the method as an applicable tool for routine urban monitoring. In addition, the proposed multiindex model is essentially an effective scene representation method, which has the potential for solving the semantic gap between the low-level features and the high-level semantics. Therefore, it can be further developed for processing other scene-based image interpretation tasks, e.g., scene classification [47]–[49], content-based image retrieval [50], and complex pattern recognition [51]–[53].

ACKNOWLEDGMENT

REFERENCES

[1] M. Hussain, D. Chen, A. Cheng, H. Wei, and D. Stanley, "Change detection from remotely sensed images: From pixel-based to object-based approaches," *ISPRS J. Photogramm. Remote Sens.*, vol. 80, pp. 91–106, Jun. 2013.

[2] P. Coppin, I. Jonckheere, K. Nackaerts, B. Muys, and E. Lambin, "Digital change detection methods in ecosystem monitoring: A review," *Int. J. Remote Sens.*, vol. 25, no. 9, pp. 1565–1596, May 2004.

[3] X. Huang and L. Zhang, "An SVM ensemble approach combining spectral, structural, and semantic features for the classification of high-resolution remotely sensed imagery," *IEEE Trans. Geosci. Remote Sens.*, vol. 51, no. 1, pp. 257–272, Jan. 2013.

[4] V. Walter, "Object-based classification of remote sensing data for change detection," *ISPRS J. Photogramm. Remote Sens.*, vol. 58, no. 3/4, pp. 225–238, Jan. 2004.

[5] T. Celik and K.-K. Ma, "Multitemporal image change detection using undecimated discrete wavelet transform and active contours," *IEEE Trans. Geosci. Remote Sens.*, vol. 49, no. 2, pp. 706–716, Feb. 2011.

[6] T. Celik, "Multiscale change detection in multitemporal satellite images," *IEEE Geosci. Remote Sens. Lett.*, vol. 6, no. 4, pp. 820–824, Oct. 2009.

[7] M. Dalla Mura, J. A. Benediktsson, F. Bovolo, and L. Bruzzone, "An unsupervised technique based on morphological filters for change detection in very high resolution images," *IEEE Geosci. Remote Sens. Lett.*, vol. 5, no. 3, pp. 433–437, Jul. 2008.

[8] M. Volpi, D. Tuia, F. Bovolo, M. Kanevski, and L. Bruzzone, "Supervised change detection in VHR images using contextual information and support vector machines," *Int. J. Appl. Earth Observ. Geoinf.*, vol. 20, pp. 77–85, Feb. 2013.

[9] Z. Lei, T. Fang, H. Huo, and D. Li, "Bi-temporal texton forest for land cover transition detection on remotely sensed imagery," *IEEE Trans. Geosci. Remote Sens.*, vol. 52, no. 2, pp. 1227–1237, Feb. 2014.

[10] X. Huang, Q. Lu, and L. Zhang, "A multi-index learning approach for classification of high-resolution remotely sensed images over urban areas," *ISPRS J. Photogramm. Remote Sens.*, vol. 90, pp. 36–48, Apr. 2014.

[11] G. Camps-Valls, L. Gómez-Chova, J. Muñoz-Marí, J. L. Rojo-Álvarez, and M. Martínez-Ramón, "Kernel-based framework for multitemporal and multisource remote sensing data classification and change detection," *IEEE Trans. Geosci. Remote Sens.*, vol. 46, no. 6, pp. 1822–1835, Jun. 2008.

[12] K. Chen, C. Huo, Z. Zhou, H. Lu, and J. Cheng, "Semi-supervised change detection via Gaussian processes," in *Proc. IEEE IGARSS*, 2009, pp. II-996–II-999.

[13] M. Roy, S. Ghosh, and A. Ghosh, "A novel approach for change detection of remotely sensed images using semi-supervised multiple classifier system," *Inf. Sci.*, vol. 269, pp. 35–47, Jun. 2014.

[14] S. Ghosh, M. Roy, and A. Ghosh, "Semi-supervised change detection using modified self-organizing feature map neural network," *Appl. Soft Comput.*, vol. 15, pp. 1–20, Feb. 2014.

[15] U. C. Benz, P. Hofmann, G. Willhauck, I. Lingenfelder, and M. Heynen, "Multi-resolution, object-oriented fuzzy analysis of remote sensing data for GIS-ready information," *ISPRS J. Photogramm. Remote Sens.*, vol. 58, no. 3/4, pp. 239–258, Jan. 2004.

[16] F. Bovolo, "A multilevel parcel-based approach to change detection in very high resolution multitemporal images," *IEEE Geosci. Remote Sens. Lett.*, vol. 6, no. 1, pp. 33–37, Jan. 2009.

[17] N. Falco, M. D. Mura, F. Bovolo, J. A. Benediktsson, and L. Bruzzone, "Change detection in VHR images based on morphological attribute profiles," *IEEE Geosci. Remote Sens. Lett.*, vol. 10, no. 3, pp. 636–640, May 2013.

[18] F. Pacifici and F. Del Frate, "Automatic change detection in very high resolution images with pulse-coupled neural networks," *IEEE Geosci. Remote Sens. Lett.*, vol. 7, no. 1, pp. 58–62, Jan. 2010.

[19] S. Liu, L. Bruzzone, F. Bovolo, and P. Du, "Hierarchical unsupervised change detection in multitemporal hyperspectral images," *IEEE Trans. Geosci. Remote Sens.*, vol. 53, no. 1, pp. 244–260, Jan. 2015.

[20] X. Huang and L. Zhang, "A multidirectional and multiscale morphological index for automatic building extraction from multispectral GeoEye-1 imagery," *Photogramm. Eng. Remote Sens.*, vol. 77, no. 7, pp. 721–732, Jul. 2011.

[21] X. Huang and L. Zhang, "Morphological building/shadow index for building extraction from high-resolution imagery over urban areas," *IEEE J. Sel. Topics Appl. Earth Observ. Remote Sens.*, vol. 5, no. 1, pp. 161–172, Feb. 2012.

[22] M. Pesaresi, A. Gerhardinger, and F. Kayitakire, "A robust built-up area presence index by anisotropic rotation-invariant textural measure," *IEEE*

J. Sel. Topics Appl. Earth Observ. Remote Sens., vol. 1, no. 3, pp. 180–192, Sep. 2008.

[23] M. Pesaresi and J. A. Benediktsson, "A new approach for the morphological segmentation of high-resolution satellite imagery," *IEEE Trans. Geosci. Remote Sens.*, vol. 39, no. 2, pp. 309–320, Feb. 2001.

[24] J. A. Benediktsson, M. Pesaresi, and K. Amason, "Classification and feature extraction for remote sensing images from urban areas based on morphological transformations," *IEEE Trans. Geosci. Remote Sens.*, vol. 41, no. 9, pp. 1940–1949, Sep. 2003.

[25] N. M. Mattikalli, "Soil color modeling for the visible and near-infrared bands of Landsat sensors using laboratory spectral measurements," *Remote Sens. Environ.*, vol. 59, no. 1, pp. 14–28, Jan. 1997.

[26] A. Huete *et al.*, "Overview of the radiometric and biophysical performance of the MODIS vegetation indices," *Remote Sens. Environ.*, vol. 83, no. 1/2, pp. 195–213, Nov. 2002.

[27] C. A. Pickett-Heaps *et al.*, "Evaluation of six satellite-derived Fraction of Absorbed Photosynthetic Active Radiation (FAPAR) products across the Australian continent," *Remote Sens. Environ.*, vol. 140, pp. 241–256, Jan. 2014.

[28] S. McFeeters, "The use of the normalized difference water index (NDWI) in the delineation of open water features," *Int. J. Remote Sens.*, vol. 17, no. 7, pp. 1425–1432, Mar. 1996.

[29] S. H. Boles *et al.*, "Land cover characterization of Temperate East Asia using multi-temporal VEGETATION sensor data," *Remote Sens. Environ.*, vol. 90, no. 4, pp. 477–489, Apr. 2004.

[30] X.-L. Chen, H.-M. Zhao, P.-X. Li, and Z.-Y. Yin, "Remote sensing image-based analysis of the relationship between urban heat island and land use/cover changes," *Remote Sens. Environ.*, vol. 104, no. 2, pp. 133–146, Sep. 2006.

[31] C. Pratola, F. Del Frate, G. Schiavon, and D. Solimini, "Toward fully automatic detection of changes in suburban areas from VHR SAR images by combining multiple neural-network models," *IEEE Trans. Geosci. Remote Sens.*, vol. 51, no. 4, pp. 2055–2066, Apr. 2013.

[32] H. Chuanwei, S. Bing, C. Yong, and Z. Meimei, "Community structure and plant diversity of secondary forests in Shenzhen," *J. Nanjing Forestry Univ. (Natural Science Edition)*, vol. 33, no. 5, pp. 21–26, 2009.

[33] M. Molinier, J. Laaksonen, and T. Hame, "Detecting man-made structures and changes in satellite imagery with a content-based information retrieval system built on self-organizing maps," *IEEE Trans. Geosci. Remote Sens.*, vol. 45, no. 4, pp. 861–874, Apr. 2007.

[34] T. Fawcett, "An introduction to ROC analysis," *Pattern Recognit. Lett.*, vol. 27, no. 8, pp. 861–874, Jun. 2006.

[35] W. J. Youden, "Index for rating diagnostic tests," *Cancer*, vol. 3, no. 1, pp. 32–35, Jan. 1950.

[36] N. Otsu, "A threshold selection method from gray-level histograms," *IEEE Trans. Syst., Man, Cybern.*, vol. SMC-9, no. 1, pp. 62–66, Jan. 1979.

[37] J. Im, J. Jensen, and J. Tullis, "Object-based change detection using correlation image analysis and image segmentation," *Int. J. Remote Sens.*, vol. 29, no. 2, pp. 399–423, Jan. 2008.

[38] A. D. Brink and N. E. Pendock, "Minimum cross-entropy threshold selection," *Pattern Recognit.*, vol. 29, no. 1, pp. 179–188, Jan. 1996.

[39] A. Baraldi and F. Parmiggiani, "An investigation of the textural characteristics associated with gray level cooccurrence matrix statistical parameters," *IEEE Trans. Geosci. Remote Sens.*, vol. 33, no. 2, pp. 293–304, Mar. 1995.

[40] R. M. Haralick, K. Shanmugam, and I. H. Dinstein, "Textural features for image classification," *IEEE Trans. Syst., Man, Cybern.*, vol. SMC-3, no. 6, pp. 610–621, Nov. 1973.

[41] X. Huang, L. Zhang, and P. Li, "Classification and extraction of spatial features in urban areas using high-resolution multispectral imagery," *IEEE Geosci. Remote Sens. Lett.*, vol. 4, no. 2, pp. 260–264, Apr. 2007.

[42] Y. O. Ouma, J. Tetuko, and R. Tateishi, "Analysis of co-occurrence and discrete wavelet transform textures for differentiation of forest and non-forest vegetation in very-high-resolution optical-sensor imagery," *Int. J. Remote Sens.*, vol. 29, no. 12, pp. 3417–3456, Jun. 2008.

[43] M. Dalla Mura, J. Atli Benediktsson, B. Waske, and L. Bruzzone, "Extended profiles with morphological attribute filters for the analysis of hyperspectral data," *Int. J. Remote Sens.*, vol. 31, no. 22, pp. 5975–5991, Dec. 2010.

[44] P. R. Marpu *et al.*, "Classification of hyperspectral data using extended attribute profiles based on supervised and unsupervised feature extraction techniques," *Int. J. Image Data Fusion*, vol. 3, no. 3, pp. 269–298, Sep. 2012.

[45] P. Blanchart and M. Datcu, "A semi-supervised algorithm for auto-annotation and unknown structures discovery in satellite image databases," *IEEE J. Sel. Topics Appl. Earth Observ. Remote Sens.*, vol. 3, no. 4, pp. 698–717, Dec. 2010.

[46] D. Bratasanu, I. Nedelcu, and M. Datcu, "Bridging the semantic gap for satellite image annotation and automatic mapping applications," *IEEE J. Sel. Topics Appl. Earth Observ. Remote Sens.*, vol. 4, no. 1, pp. 193–204, Mar. 2011.

[47] N. Rasiwasia and N. Vasconcelos, "Scene classification with low-dimensional semantic spaces and weak supervision," in *Proc. IEEE CVPR*, 2008, pp. 1–6.

[48] A. Bolovinou, I. Pratikakis, and S. Perantonis, "Bag of spatio-visual words for context inference in scene classification," *Pattern Recognit.*, vol. 46, no. 3, pp. 1039–1053, Mar. 2013.

[49] S. Aksoy, K. Koperski, C. Tusk, G. Marchisio, and J. C. Tilton, "Learning Bayesian classifiers for scene classification with a visual grammar," *IEEE Trans. Geosci. Remote Sens.*, vol. 43, no. 3, pp. 581–589, Mar. 2005.

[50] Y. Liu, D. Zhang, G. Lu, and W.-Y. Ma, "A survey of content-based image retrieval with high-level semantics," *Pattern Recognit.*, vol. 40, no. 1, pp. 262–282, Jan. 2007.

[51] C.-C. Huang, S.-J. Wang, Y.-J. Chang, and T. Chen, "A Bayesian hierarchical detection framework for parking space detection," in *Proc. IEEE ICASSP*, 2008, pp. 2097–2100.

[52] R. R. Vatsavai, A. Cheriyadat, and S. Gleason, "Unsupervised semantic labeling framework for identification of complex facilities in high-resolution remote sensing images," in *Proc. IEEE ICDMW*, 2010, pp. 273–280.

[53] S. Aksoy, H. G. Akcay, and T. Wassenaar, "Automatic mapping of linear woody vegetation features in agricultural landscapes using very high resolution imagery," *IEEE Trans. Geosci. Remote Sens.*, vol. 48, no. 1, pp. 511–522, Jan. 2010.
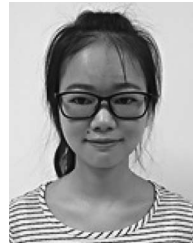
Dawei Wen received the B.S. degree in surveying and mapping from Wuhan University, Wuhan, China, in 2013. She is currently working toward the Ph.D. degree in photogrammetry and remote sensing in the State Key Laboratory of Information Engineering in Surveying, Mapping and Remote Sensing, Wuhan University.

Her research interests include change analysis of multitemporal remote sensing images and remote sensing applications.
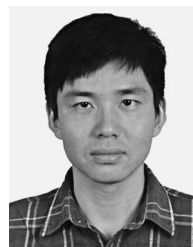
Xin Huang (M'13–SM'14) received the Ph.D. degree in photogrammetry and remote sensing from Wuhan University, Wuhan, China, in 2009, working in the State Key Laboratory of Information Engineering in Surveying, Mapping and Remote Sensing (LIESMARS).

Since 2012, he has been a Full Professor with LIESMARS, Wuhan University. He has authored or coauthored over 60 peer-reviewed articles in international journals. His research interests include hyperspectral data analysis, high-resolution image processing, pattern recognition, and remote sensing applications.

Prof. Huang was the Lead Guest Editor of the special issue on information extraction from high-spatial-resolution optical remotely sensed imagery of the IEEE JOURNAL OF SELECTED TOPICS IN APPLIED EARTH OBSERVATIONS AND REMOTE SENSING (vol. 8, no. 5, May 2015). Since 2014, he has served as an Associate Editor of the IEEE GEOSCIENCE AND REMOTE SENSING LETTERS. He was the recipient of the Top Ten Academic Star of Wuhan University in 2009, the Boeing Award for the Best Paper in Image Analysis and Interpretation from the American Society for Photogrammetry and Remote Sensing in 2010, the New Century Excellent Talents in University from the Ministry of Education of China in 2011, the National Excellent Doctoral Dissertation Award of China in 2012, and the China National Science Fund for Excellent Young Scholars in 2015. In 2011, he was recognized by the IEEE Geoscience and Remote Sensing Society (GRSS) as a Best Reviewer of the IEEE GEOSCIENCE AND REMOTE SENSING LETTERS. He was the winner of the IEEE GRSS 2014 Data Fusion Contest.

This article has been accepted for inclusion in a future issue of this journal. Content is final as presented, with the exception of pagination.

WEN *et al.*: CHANGE DETECTION METHOD FOR URBAN HIGH-RESOLUTION REMOTELY SENSED IMAGERY

17

Liangpei Zhang (M'06–SM'08) received the B.S. degree in physics from Hunan Normal University, Changsha, China, in 1982, the M.S. degree in optics from the Chinese Academy of Sciences, Xian, China, in 1988, and the Ph.D. degree in photogrammetry and remote sensing from Wuhan University, Wuhan, China, in 1998.

He is currently the Head of the Remote Sensing Division, State Key Laboratory of Information Engineering in Surveying, Mapping and Remote Sensing, Wuhan University. He is also a Chang Jiang Scholar Chair Professor appointed by the Ministry of Education of China. He is currently a Principal Scientist for the China State Key Basic Research Project (2011–2016) appointed by the Ministry of National Science and Technology of China to lead the remote sensing program in China. He has over 300 research papers. He is the holder of five patents. His research interests include hyperspectral remote sensing, high-resolution remote sensing, image processing, and artificial intelligence.

Dr. Zhang is a Fellow of the Institution of Engineering and Technology, an Executive Member (Board of Governor) of the China National Committee of the International Geosphere-Biosphere Programme, and an Executive Member of the China Society of Image and Graphics. He regularly serves as a Cochair of the series SPIE Conferences on Multispectral Image Processing and Pattern Recognition, the Conference on Asia Remote Sensing, and many other conferences. He edits several conference proceedings, issues, and geoinformatics symposiums. He also serves as an Associate Editor of the *International Journal of Ambient Computing and Intelligence*, the *International Journal of Digital Multimedia Broadcasting*, the *Journal of Geo-spatial Information Science*, the *Journal of Remote Sensing*, and the IEEE TRANSACTIONS ON GEOSCIENCE AND REMOTE SENSING.

Jón Atli Benediktsson (S'84–M'90–SM'99–F'04) received the Cand.Sci. degree in electrical engineering from the University of Iceland, Reykjavik, Iceland, in 1984 and the M.S.E.E. and Ph.D. degrees from Purdue University, West Lafayette, IN, USA, in 1987 and 1990, respectively.

He is currently a Rector and a Professor of electrical and computer engineering with the University of Iceland. He is a Cofounder of the biomedical startup company Oxymap. His research interests are in remote sensing, biomedical analysis of signals, pattern recognition, image processing, and signal processing. He has published extensively in those fields.

Prof. Benediktsson is a Fellow of the International Society for Optics and Photonics and a member of the Association of Chartered Engineers in Iceland (VFI) and Societas Scinetiarum Islandica. He was the 2011–2012 President of the IEEE Geoscience and Remote Sensing Society (GRSS) and has been on the GRSS Administrative Committee since 2000. He was an Editor of the IEEE TRANSACTIONS ON GEOSCIENCE AND REMOTE SENSING (TGRS) from 2003 to 2008 and has served as an Associate Editor of TGRS since 1999, the IEEE GEOSCIENCE AND REMOTE SENSING LETTERS since 2003, and IEEE ACCESS since 2013. He is on the International Editorial Board of the *International Journal of Image and Data Fusion* and was the Chairman of the Steering Committee of the IEEE JOURNAL OF SELECTED TOPICS IN APPLIED EARTH OBSERVATIONS AND REMOTE SENSING in 2007–2010. He was a recipient of the Stevan J. Kristof Award from Purdue University in 1991 as outstanding graduate student in remote sensing, the Icelandic Research Council's Outstanding Young Researcher Award in 1997, and the IEEE Third Millennium Medal in 2000. He was a corecipient of the University of Iceland's Technology Innovation Award in 2004. He was also a recipient of the yearly research award from the Engineering Research Institute of the University of Iceland in 2006, the Outstanding Service Award from the IEEE Geoscience and Remote Sensing Society in 2007, and the IEEE/VFI Electrical Engineer of the Year Award in 2013. He was also a corecipient of the 2012 IEEE TRANSACTIONS ON GEOSCIENCE AND REMOTE SENSING Paper Award and the IEEE GRSS Highest Impact Paper Award in 2013. He is also a member of Tau Beta Pi.